Angewandte Chemie
Eine Zeitschrift der Gesellschaft Deutscher Chemiker

Supporting Information

Conservation of Nickel Ion Single-Active Site Character in a Bottom-Up Constructed π-Conjugated Molecular Network

D. Baranowski, I. Cojocariu, A. Sala, C. Africh, G. Comelli, L. Schio, M. Tormen, L. Floreano, V. Feyer*, C. M. Schneider*

Supporting Information

Conservation of Nickel Ion Single-Active Site Character in a Bottom-Up Constructed π-Conjugated Molecular Network

Daniel Baranowski [a,], Iulia Cojocariu [a], Alessandro Sala [b], Cristina Africh [b], Giovanni Comelli [b,c], Luca Schio [b], Massimo Tormen [b], Luca Floreano [b], Vitaliy Feyer [a,d,*] and Claus Michael Schneider [a,d,e]*

[a]*Peter Grünberg Institute (PGI-6), Jülich Research Centre, 52428 Jülich, Germany*
[b]*TASC Laboratory, CNR-IOM, 34149 Trieste, Italy*
[c]*Department of Physics, University of Trieste, 34127 Trieste, Italy*
[d]*Faculty of Physics and Center for Nanointegration Duisburg-Essen (CENIDE), University of Duisburg-Essen, 47048 Duisburg, Germany*
[e]*Department of Physics and Astronomy, UC Davis, Davis, CA 95616, USA*
*Corresponding authors: d.baranowski@fz-juelich.de, v.feyer@fz-juelich.de

Table of Contents

1. Experimental Section

The clean Au(111) and Ag(111) substrates were prepared using the standard procedure of repeated cycles of Ar^+ sputtering at 2 keV followed by subsequent annealing to 800 K. NiTBrPP molecules (Frontier Scientific) were evaporated at 660 K from a Knudsen cell type evaporator with the Au(111) and Ag(111) substrates held at room temperature. At the NanoESCA beamline of Elettra, the Italian synchrotron facility in Trieste, the coverage was checked by means of low-energy electron diffraction, while defining the saturated coverage by the appearance of sharp diffraction spots that vanish upon exceeding the ideal coverage regime. When performing the STM measurements the coverage was directly estimated from the images obtained, while at the ALOISA beamline of Elettra a quartz microbalance was used.

Valence band photoelectron spectroscopy was performed at the NanoESCA beamline. A detailed description of the installed electrostatic PEEM setup can be found elsewhere.[1] The base pressure was lower than $5 \cdot 10^{-11}$ mbar with the sampled thermalized at 90 K before measuring at a photon energy of 30 eV at a total energy resolution of 100 meV. Thereby, continuously rastering of the sample was applied in order to avoid beam-induced damage and desorption of the molecular layer.

STM/STS data were obtained using an Omicron low-temperature apparatus located at the CNR-IOM Materials Foundry institute in Trieste, Italy. The images were recorded at 77 K while applying an inverse bias voltage to the electrochemically etched tungsten tip with the sample grounded. When performing measurements, the base pressure was below $7 \cdot 10^{-11}$ mbar. Spectroscopy measurement were obtained with a lock-in amplifier generating a carrier wave of amplitude 20 mV and frequency 1090 Hz.

Core level photoelectron and absorption spectroscopy measurements were conducted at the ALOISA beamline that is also located at the Elettra synchrotron at a base pressure below $1 \cdot 10^{-10}$ mbar.[2] Photoelectron spectroscopy data were acquired in normal emission geometry in p-polarization with a 4° grazing angle of linearly-polarized light beam with respect to the surface plane. Binding energies were calibrated with the bulk-sensitive Au 4f main line located at 84 eV.[3] Ni 2p spectra were collected at 1050 eV with a total energy resolution of 450 meV while C 1s, N 1s and Br 3d spectra were recorded at 515 eV with a total energy resolution of 160 meV. Near-edge x-ray absorption fine structure spectra were acquired in partial electron yield mode by means of a channeltron multiplier equipped with a negatively biased grid to filter out low energy secondary electrons, in order to increase the signal to background ratio. To investigate the sample dichroism, the absorption spectra were collected at two different orientations of the surface with respect to the linear polarization vector of the photon beam, namely transverse magnetic (TM, closely p-polarization) and transverse electric (TE, s-polarization) geometry, by sample rotation around the photon beam axis, thus allowing us to discriminate between π*- and σ*-symmetry resonances. The light grazing angle was kept constant at 6°. The photon flux normalization and the energy calibration procedures are described elsewhere.[4]

2. Temperature Optimization on Au(111)

Br 3d photoelectron spectra obtained for the parent NiTBrPP/Au(111) system together with those after the thermal treatments at 473 K and 673 K, are summarized in Figure S1. The as-deposited molecular layer exhibits a doublet with the Br $3d_{5/2}$ main line at a binding energy of 69.9 eV, which is characteristic for carbon-bound Br species. The signal corresponding to the brominated porphyrin precursor is reduced as a consequence of annealing the sample to 473 K. Consequently, an additional doublet that can be attributed to Br species adsorbed on the Au(111) substrate after activation of the brominated porphyrin units arises at lower binding energies.[5–7] Annealing to 673 K, finally, resulted in all Br species to desorb from the substrate. Direct annealing to this temperature was subsequently chosen to produce a covalent porphyrin network starting from a saturated NiTBrPP layer on Au(111).

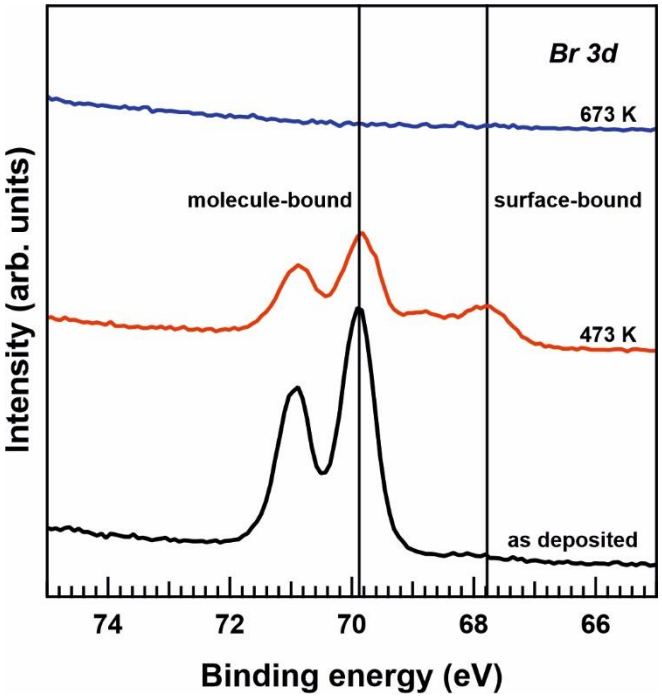

***Figure S1*:** Br 3d photoelectron spectra recorded at a photon energy of 515 eV (p-polarization) in normal emission displaying the changes observed upon stepwise annealing of the pristine NiTBrPP layer on Au(111).

3. Supplementary Figures

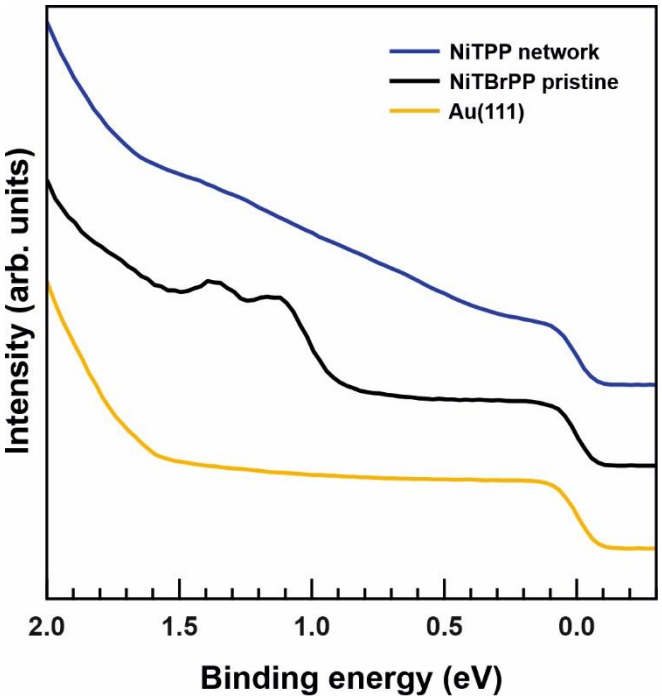

***Figure S2*:** Angle-integrated valence band spectra recorded at a photon energy of 30 eV using p-polarized light at the different preparation steps indicated within the legend.

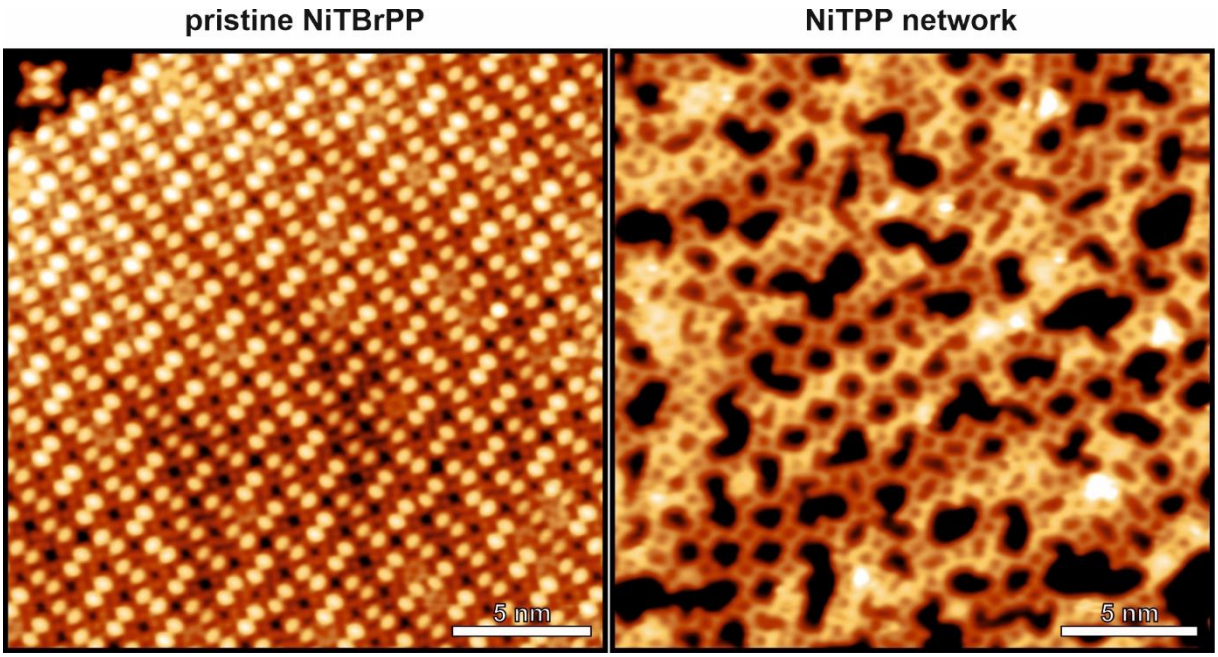

***Figure S3*:** Comparison of the topographic STM images highlighting the changes when annealing the pristine NiTBrPP layer on Au(111) (left, V = -1.8 V, I = 0.5 nA) to 673 K that induces the formation of NiTPP-based covalent network (right, V = -0.4 V, I = 0.5 nA).

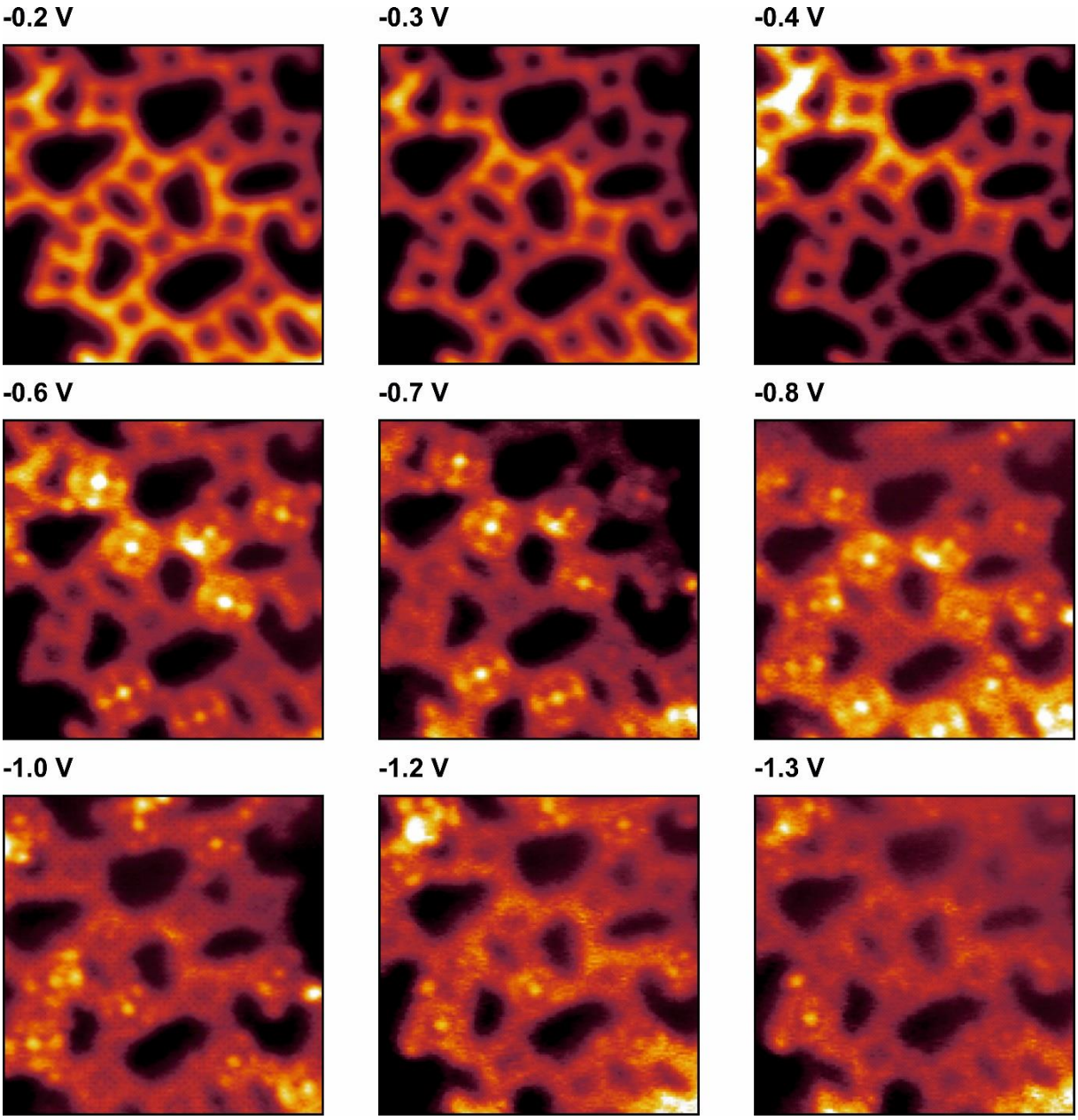

***Figure S4*:** Overview presenting different 32x32 nm d*I*/d*V* maps obtained across the occupied states of covalent NiTPP-based network with the respective bias applied indicated in the caption.

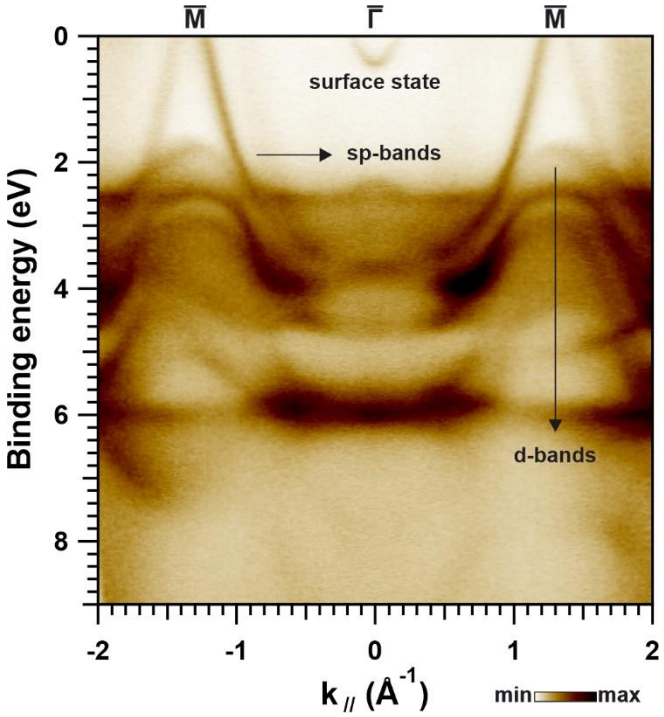

***Figure S5*:** Photoelectron $k_{//}$ distribution of bare Au(111) along the substrate $\bar{M}$-$\bar{\Gamma}$-$\bar{M}$ direction recorded at a photon energy of 30 eV using p-polarized light.

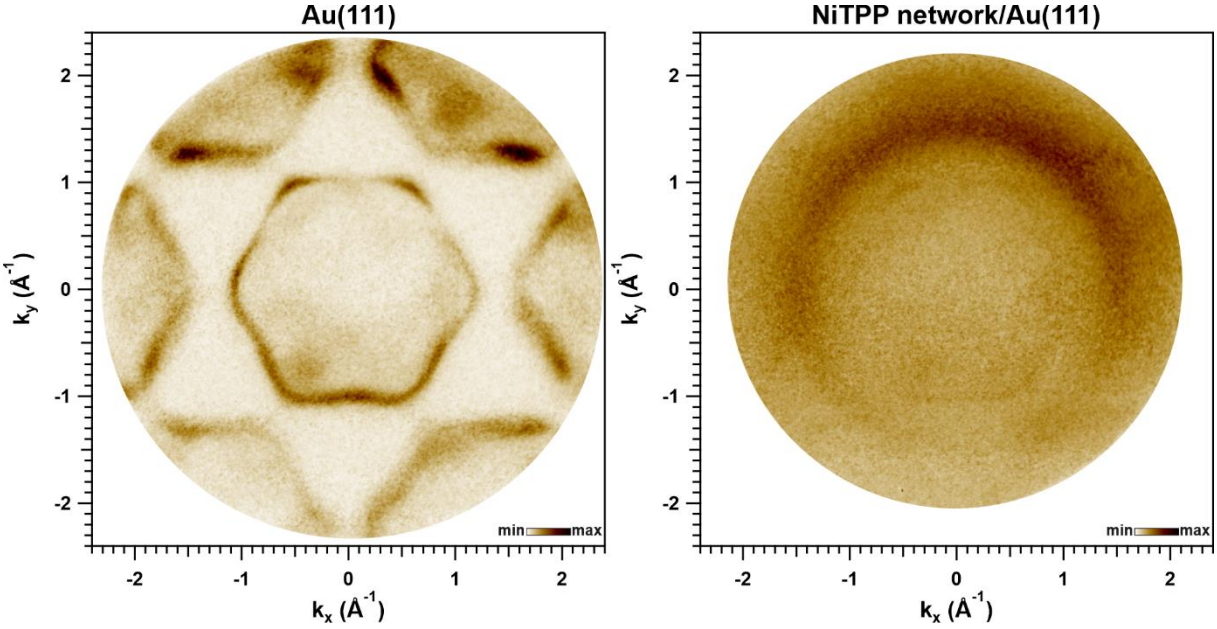

***Figure S6*:** Constant binding energy (1 eV) momentum images of bare Au(111) (left) and after formation of NiTPP-based network on Au(111) (right) recorded at a photon energy of 30 eV using p-polarized light. The top-bottom asymmetry in intensity is caused by the angle of incidence (25° with respect to the surface) of the beam.

4. X-ray Photoelectron Spectroscopy Characterization of the Chemical Changes upon Creation of Covalent NiTPP-Based Network on Au(111)

Figure S6 is comparing the C 1s photoelectron spectra of the parent NiTBrPP layer and the covalent NiTPP network. The multicomponent signal of pristine NiTBrPP is transformed upon Ullmann coupling of activated precursor molecules. In particular, the C-Br contribution at high binding energy (indicated by the arrow at ~285.2 eV) vanishes and the main carbon peak displays an overall shift to lower binding energy (~0.2 eV) together with a decrease of the energy spread among different carbon atoms.[8] This fully supports the picture of a more uniform carbon environment within an extended covalent nanostructure characterized by π-conjugation.

Figure S7 and S8 present a comparison of the N 1s and Ni $2p_{3/2}$ core-level photoelectron lines before and after polymerization. In both cases, the covalent linking of activated NiTBrPP units does not alter either the spectral shape or linewidth. The overall reduced intensity can be attributed to the partial desorption of molecular precursor units. Yet, the signals are shifted by ~0.2 eV towards higher binding energies (opposite to the case of the C 1s signal) after the formation of the covalent NiTPP network. The flattening of all molecular constituents (i.e. the pyrrolic macrocycle and the phenyl groups) is expected to influence the distance of the functional center to the supporting interface, which can explain these shifts as a result of changed core hole screening as reported for various on-surface reactions.[8,9] Most importantly, the Ni cores remain coordinated within the porphyrin polymer, also retaining the pristine single-molecule Ni(II) oxidation state.[10]

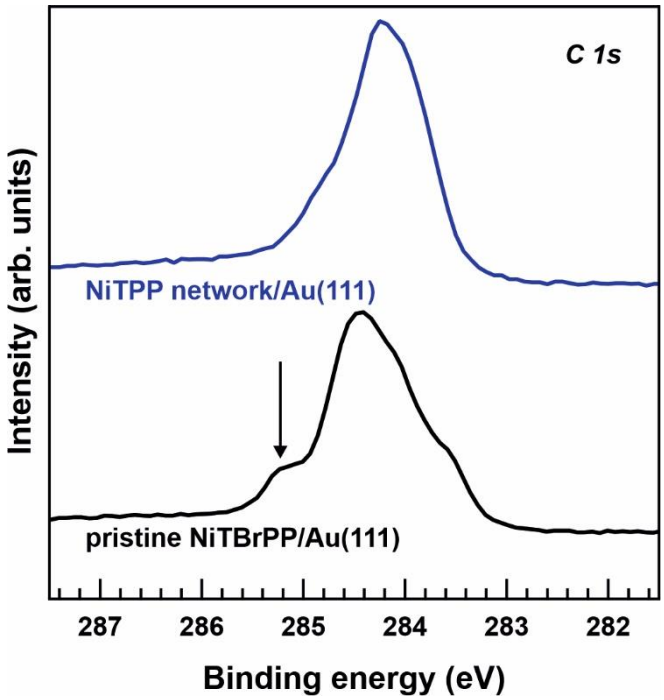

***Figure S7*:** Overview of the C 1s photoelectron spectra recorded at a photon energy of 515 eV (p-polarization) in normal emission corresponding to pristine NiTBrPP and NiTPP-based network on Au(111).

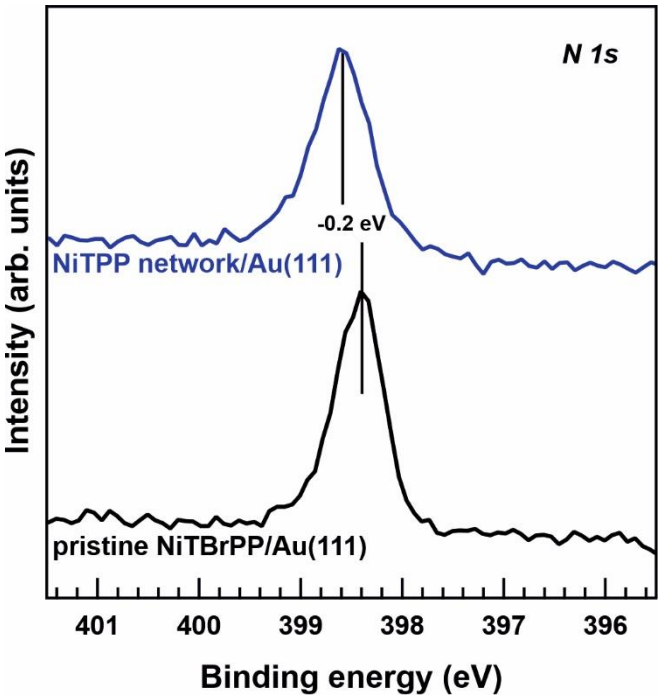

***Figure S8*:** Overview of the N 1s photoelectron spectra recorded at a photon energy of 515 eV (p-polarization) in normal emission corresponding to pristine NiTBrPP and NiTPP-based network on Au(111).

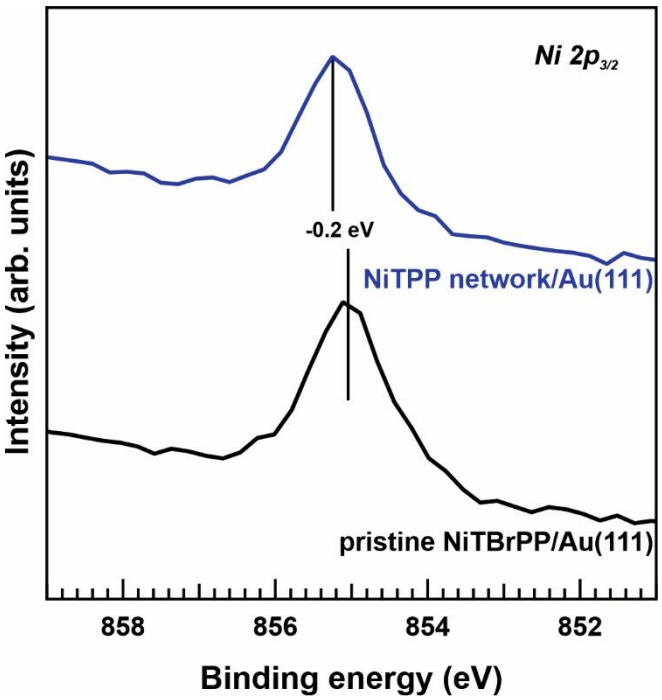

***Figure S9*:** Overview of the Ni $2p_{3/2}$ photoelectron spectra recorded at a photon energy of 1050 eV (p-polarization) in normal emission corresponding to pristine NiTBrPP and NiTPP-based network on Au(111).

5. Covalent NiTPP-based Network on Ag(111)

We also explored the more reactive Ag(111) substrate as a catalyst to create covalent NiTPP-based network. We performed the polymerization reaction by direct annealing to 573 K starting from a saturated layer of NiTBrPP on Ag(111). Figure S9 compares the parallel momentum $k_{//}$ versus binding energy dependence along the substrate $\bar{M}$-$\bar{\Gamma}$-$\bar{M}$ direction characteristic for both Ag(111) and NiTPP network on Ag(111) recorded at a photon energy of 30 eV using p-polarized light. The parabola of states appears to be also exhibited by the covalent nanomesh created on Ag(111). The parabola obtained on Ag(111) substrate is also highlighted in blue and compared (green) with the bottom part of the parabola obtained on Au(111) in Figure S9 (right). It can be concluded that the more pronounced charge transfer at the Ag(111) interface results in shift of the parabola of ~0.6 eV towards higher binding energies while the shape remains equal. Similar findings were obtained when creating graphene at more reactive interfaces.[11]

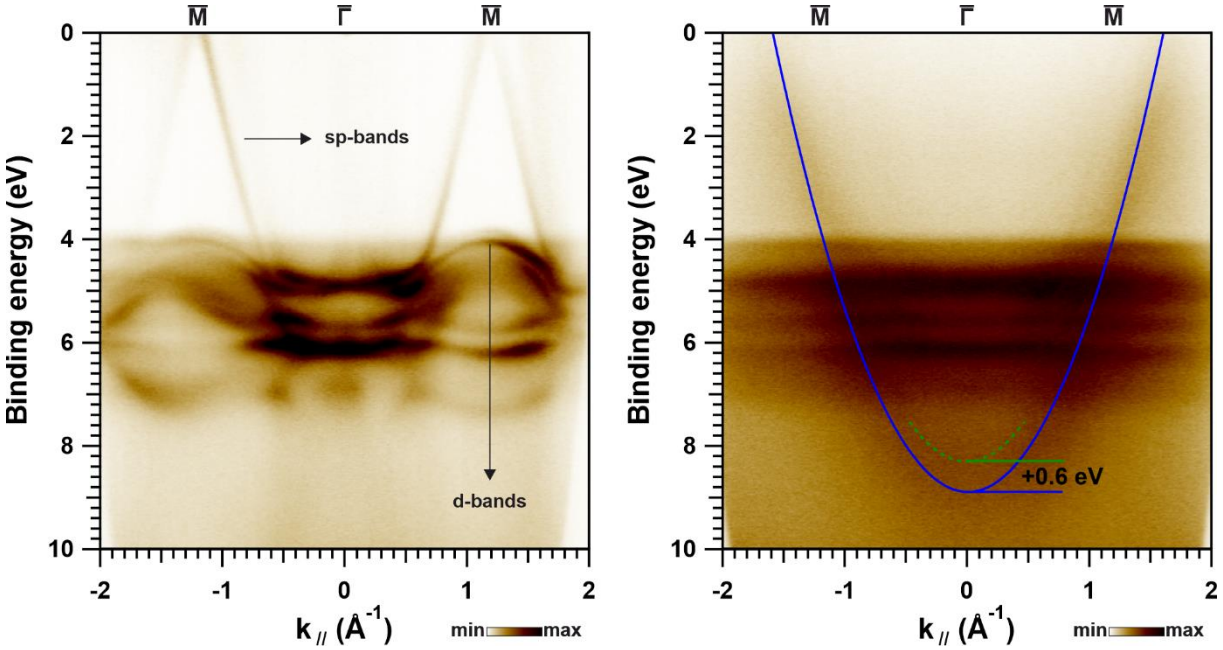

Figure S10: Photoelectron $k_{//}$ distribution of bare Ag(111) (left) and after the formation of the NiTPP-based network on Ag(111) (right) with the parabola highlighted in blue and compared with the bottom part (green) of the parabola obtained for NiTPP-based network on Au(111) along the substrate $\bar{M}$-$\bar{\Gamma}$-$\bar{M}$ direction recorded at a photon energy of 30 eV using p-polarized light.

Figure S10 further summarizes the near-edge x-ray absorption fine structure spectra corresponding to pristine NiTBrPP layer and NiTPP network on Ag(111). Similar to the case of Au(111) the C K-edge spectra reflect the transition from discrete molecular levels to a continuum of states upon polymerization where the phenyl substituents are forced into a flat configuration with the details discussed in the main text. The differences in the N K-edge spectrum of the parent NiTBrPP layer and covalent nanomesh on Au(111) are also apparent in the case of Ag(111). The energy position of the low energy π*-resonance is shifted with respect to the one of the σ*-resonance while the high energy π*-resonances are broadened. After the formation of covalent NiTPP network all transitions are shifted towards lower photon energies and reduced

in intensity. This phenomenon is well-described and indicates an increase in the charge transfer from the substrate that can be related to the formation of the planar covalent nanomesh that is more influenced on the more reactive Ag(111) substrate.[12,13] Most importantly, the coordination characteristics of the N-moiety can be summarized to be unaltered. This is further confirmed by the Ni L_3-edge spectra. The shift of ~0.1 eV towards lower photon energies upon NiTPP network formation can be attributed to the increased charge transfer from the substrate that compensates the opposite shift related to the increased Ni to N-backbonding observed on Au(111). Again, no changes in the spectral shape and satellite structure are evident. This allows concluding single-active site character conservation can be extended to more reactive interfaces, which undermines the multifunctionality of the covalent nanomesh. The covalent backbone and functional transition metal center are tuned by the charge transfer at the interface but remain distinct constituents.

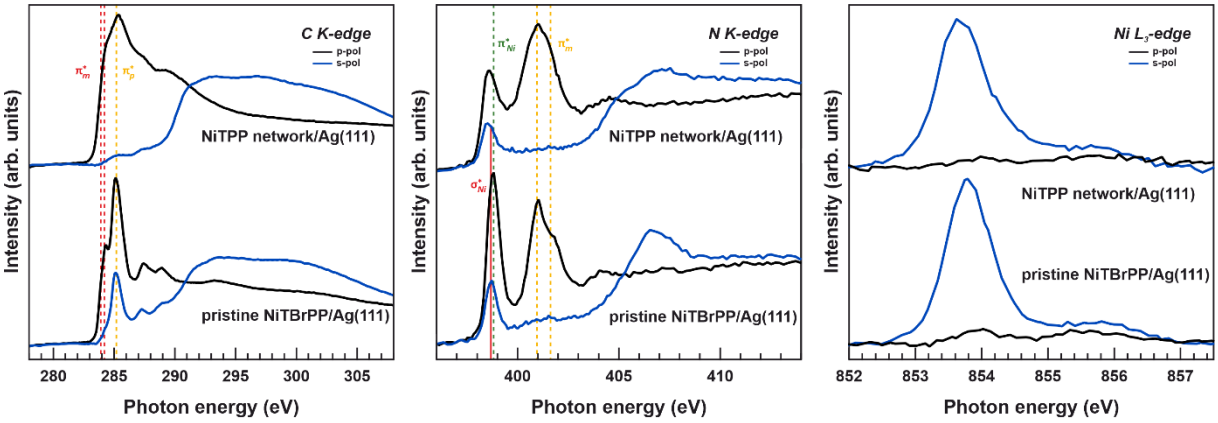

***Figure S11*:** Near-edge x-ray absorption fine structure spectra recorded across the C K-edge, N K-edge and Ni L_3-edge for both the pristine NiTBrPP layer on Ag(111) and after the formation of the NiTPP-based network.

6. References

[1] C. M. Schneider, C. Wiemann, M. Patt, V. Feyer, L. Plucinski, I. P. Krug, M. Escher, N. Weber, M. Merkel, O. Renault, N. Barrett, *J Electron Spectros Relat Phenomena* **2012**, *185*, 330–339.

[2] L. Floreano, G. Naletto, D. Cvetko, R. Gotter, M. Malvezzi, L. Marassi, A. Morgante, A. Santaniello, A. Verdini, F. Tommasini, G. Tondello, *Review of Scientific Instruments* **1999**, *70*, 3855–3864.

[3] M. T. Anthony, M. P. Seah, *Surface and Interface Analysis* **1984**, *6*, 95–106.

[4] L. Floreano, A. Cossaro, R. Gotter, A. Verdini, G. Bavdek, F. Evangelista, A. Ruocco, A. Morgante, D. Cvetko, *The Journal of Physical Chemistry C* **2008**, *112*, 10794–10802.

[5] S. A. Krasnikov, C. M. Doyle, N. N. Sergeeva, A. B. Preobrajenski, N. A. Vinogradov, Y. N. Sergeeva, A. A. Zakharov, M. O. Senge, A. A. Cafolla, *Nano Res* **2011**, *4*, 376–384.

[6] O. Plekan, V. Feyer, N. Tsud, M. Vondráček, V. Cháb, V. Matolín, K. C. Prince, *Surf Sci* **2012**, *606*, 435–443.

[7] K. A. Simonov, N. A. Vinogradov, A. S. Vinogradov, A. V. Generalov, E. M. Zagrebina, N. Mårtensson, A. A. Cafolla, T. Carpy, J. P. Cunniffe, A. B. Preobrajenski, *Journal of Physical Chemistry C* **2014**, *118*, 12532–12540.

[8] L. Smykalla, P. Shukrynau, M. Korb, H. Lang, M. Hietschold, *Nanoscale* **2015**, *7*, 4234–4241.

[9] I. Cojocariu, F. Feyersinger, P. Puschnig, L. Schio, L. Floreano, V. Feyer, C. M. Schneider, *Chemical Communications* **2021**, *57*, 3050–3053.

[10] M. Stredansky, S. Moro, M. Corva, M. Jugovac, G. Zamborlini, V. Feyer, C. M. Schneider, I. Cojocariu, H. M. Sturmeit, M. Cinchetti, A. Verdini, A. Cossaro, L. Floreano, E. Vesselli, *The Journal of Physical Chemistry C* **2020**, *124*, 6297–6303.

[11] K. V. Emtsev, F. Speck, Th. Seyller, L. Ley, J. D. Riley, *Phys Rev B* **2008**, *77*, 155303.

[12] I. Cojocariu, H. M. Sturmeit, G. Zamborlini, A. Cossaro, A. Verdini, L. Floreano, E. D'Incecco, M. Stredansky, E. Vesselli, M. Jugovac, M. Cinchetti, V. Feyer, C. M. Schneider, *Appl Surf Sci* **2020**, *504*, 144343.

[13] A. Calabrese, L. Floreano, A. Verdini, C. Mariani, M. G. Betti, *Phys Rev B* **2009**, *79*, 115446.